INTERNATIONAL JOURNAL FOR NUMERICAL METHODS IN FLUIDS
Int. J. Numer. Meth. Fluids **30**: 83–103 (1999)

FINITE ELEMENT SIMULATION OF TURBULENT COUETTE–POISEUILLE FLOWS USING A LOW REYNOLDS NUMBER k–ϵ MODEL

SIAMAK KAZEMZADEH HANNANI* AND MICHEL STANISLAS[1]

Room B-18, Laboratoire de Mécanique des Fluides, Ecole Centrale de Lille, LML CNRS-URA 1441, F59651 Villeneuve d'Ascq, France

SUMMARY

Developing Couette–Poiseuille flows at $Re = 5000$ are studied using a low Reynolds number k–ϵ two-equation model and a finite element formulation. Mesh-independent solutions are obtained using a standard Galerkin formulation and a Galerkin/least-squares stabilized method. The predictions for the velocity and turbulent kinetic energy are compared with available experimental results and to the DNS data. Second moment closure's solutions are also compared with those of the k–ϵ model. The deficiency of eddy viscosity models to predict dissymmetric low Reynolds number channel flows has been demonstrated. Copyright © 1999 John Wiley & Sons, Ltd.

KEY WORDS: k–ϵ model; Couette–Poiseuille flows; finite element method; low Reynolds number

1. INTRODUCTION

It is well-known that k–ϵ models like other turbulence closures are not valid in the viscosity affected near-wall regions. The popular wall functions method, which is based on the assumed universality of the law of the wall, avoids completely the solution of the transport equations in the wall region. However, the notion of the law of the wall and the assumption of a logarithmic universal velocity profile are in clear contradiction for flows with regions of recirculation (separation and reattachment). An alternative to using wall functions is to employ turbulence models that are valid all the way to the wall, called 'low Reynolds number' treatments or models. These models are obtained by adding extra terms to the transport equations and by introducing damping functions to take into account the change in the turbulence structure in the wall regions. In this study, the latter approach is utilized to simulate low Reynolds number turbulent Couette–Poiseuille flows.

Various low Reynolds number k–ϵ models have been proposed over the past two decades. These models can be roughly divided in two groups. The first group models are empirical ones that are introduced, before the mid 1980s, so that predictions can match the rather limited experimental data in the near-wall region. Patel *et al.* [1] studied various near-wall k–ϵ models and concluded that none was entirely successful in predicting the essential features of the flow

* Correspondence to: Room B-18, Laboratoire de Mécanique des Fluides, Ecole Centrale de Lille, LML CNRS-URA 1441, F59651 Villeneuve d'Ascq, France. Tel.: + 33 20337169; fax: + 33 20337170.
[1] E-mail: stanislas@ec-lille.fr

CCC 0271–2091/99/090083–21$17.50

Received October 1996
Revised January 1998

close to a wall, even in the relatively simple cases of two-dimensional attached steady flows. Recently, advances in direct numerical simulation (DNS) of turbulent flows have provided in the literature extensive qualitative and quantitative information on the structure of the viscous sublayer and buffer layer. Consequently, models based on the DNS results have been introduced (see e.g. Rodi and Mansour [2] and Michelassi *et al.* [3]). These models are tightly tuned by modifying model constants and damping functions to render DNS data under particular conditions (e.g. fully developed plane Poiseuille flows). In this study, Chien's [4] low Reynolds number $k-\epsilon$ version, which is an empirical model, is employed to resolve the wall region. The authors have chosen this model for the following reasons. First of all, previous numerical experiments with Chien's model to simulate channel flows (see Monnier [5] and Monnier and Stanislas [6]) have shown that this model behaves rather better than other empirical ones and is numerically more stable and robust. Secondly, in this version, the extra terms introduced to the transport equations of k and ϵ are more easily implemented using a finite element method. Other models contain terms that depend on second-order derivatives of the mean velocity. Computations are also conducted by modifying damping functions of Chien's model by those proposed by Rodi and Mansour [2], which are based on DNS data.

The overall success of all turbulence models on solving complex industrial flows depends largely on the behaviour of these models in predicting benchmark experimental flows. Unfortunately, experimental results are not always very complete. For example, inlet conditions are not well-defined and not all turbulence properties are measured. Fully developed turbulent one-dimensional Poiseuille flows are among the reference problems that have been extensively used in the literature to study the performance of different turbulence models. Today, DNS data is also used as an alternative. However, fully developed symmetric flows between fixed walls do not seem to be sufficient to provide a complete validation of models. The lack of detailed experimental results has motivated researchers to define other experimental test cases that have not only a simple geometric configuration, allowing them to be treated equally by DNS, but are also physically sufficiently complex. Recently, at the OMERA-IMFL, an experimental set-up was constructed which allows the so-called turbulent Couette–Poiseuille flows to be obtained (see Corenflos [7]). These flows are induced between two parallel plane walls by imposing a pressure gradient and the uniform motion of one of the walls. A great variety of velocity profiles can be obtained by modifying the velocity of the moving wall (Figure 1). Note that for the intermediate-type flow, the shear stress at the moving wall vanishes. The experimental set-up can be divided in two parts. In the first part, a pure (symmetric) Poiseuille flow is developed between two fixed walls that can be used as inflow boundary conditions for two-dimensional numerical computations (see Figure 2 for details). In

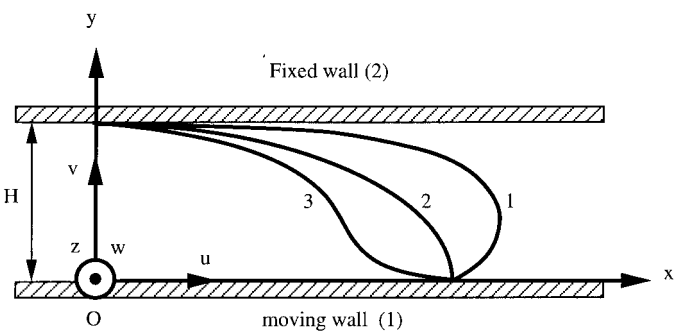

Figure 1. Couette–Poiseuille flows, 1, Poiseuille-type flow; 2, intermediate-type flow; 3, Couette-type flow.

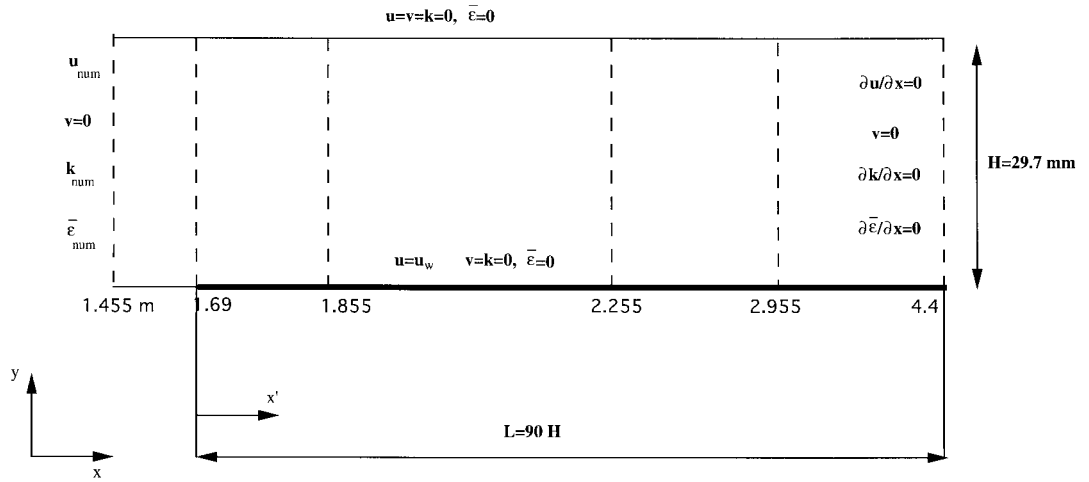

Figure 2. Domain and boundary conditions.

the second part, where one of the walls is moving, turbulent Couette–Poiseuille flows are obtained. Experiments are performed using air at a Reynolds number of 5000 based on the mean bulk velocity and the channel height. These flows have already been the subject of a Workshop [8] organized by ERCOFTAC at Karlsruhe, Germany, in 1995 for testing different turbulence models.

In this paper a finite element method is employed to study the characteristics of turbulent Couette–Poiseuille flows and to validate Chien's turbulence model for dissymmetric flows at low Reynolds numbers. The development of turbulent Couette–Poiseuille flows is another subject that is investigated in this work. Special attention is devoted to determine complete, fully developed mean velocity and turbulent kinetic energy profiles and to compare the model predictions with the experimental results at the developed sections.

Two different finite element formulations have been used in this study. Reynolds averaged Navier–Stokes equations and k–ϵ equations are discretized using a standard Galerkin finite element formulation, employing bilinear elements for all dependent variables except for the pressure. The pressure is determined using a penalty approach. To examine the influence of numerical scheme on the accuracy of the predictions, the Galerkin penalty method is replaced by a stabilized Galerkin/least-squares (GLS) formulation employing equal-order biquadratic (serendipity) velocity–pressure elements. Serendipity elements are also employed for k and ϵ variables using a standard Galerkin formulation.

2. GOVERNING EQUATIONS

The mathematical model consists of the following Reynolds averaged Navier–Stokes and continuity equations for incompressible two-dimensional flows

$$\bar{u}\frac{\partial \bar{u}}{\partial x}+\bar{v}\frac{\partial \bar{u}}{\partial y}=-\frac{1}{\rho}\frac{\partial \overline{p^*}}{\partial x}+\frac{\partial}{\partial x}\left(\nu_{\text{eff}}\frac{\partial \bar{u}}{\partial x}\right)+\frac{\partial}{\partial y}\left(\nu_{\text{eff}}\frac{\partial \bar{u}}{\partial y}\right)+\frac{\partial \nu_{\text{eff}}}{\partial x}\frac{\partial \bar{u}}{\partial x}+\frac{\partial \nu_{\text{eff}}}{\partial y}\frac{\partial \bar{v}}{\partial x}, \tag{1}$$

$$\bar{u}\frac{\partial \bar{v}}{\partial x}+\bar{v}\frac{\partial \bar{v}}{\partial y}=-\frac{1}{\rho}\frac{\partial \overline{p^*}}{\partial y}+\frac{\partial}{\partial x}\left(\nu_{\text{eff}}\frac{\partial \bar{v}}{\partial x}\right)+\frac{\partial}{\partial y}\left(\nu_{\text{eff}}\frac{\partial \bar{v}}{\partial y}\right)+\frac{\partial \nu_{\text{eff}}}{\partial x}\frac{\partial \bar{u}}{\partial y}+\frac{\partial \nu_{\text{eff}}}{\partial y}\frac{\partial \bar{v}}{\partial y}, \tag{2}$$

$$\frac{\partial \bar{u}}{\partial x}+\frac{\partial \bar{v}}{\partial y}=0, \tag{3}$$

where

$$v_{\text{eff}}=v+v_t, \tag{4}$$

$$p^*=p+\frac{2}{3}k, \tag{5}$$

$$v_t=C_\mu f_\mu \frac{k^2}{\tilde{\epsilon}}. \tag{6}$$

In Equations (1) and (2), $\bar{u}$ and $\bar{v}$ are horizontal and vertical components of the mean velocity vector respectively. p^* is a quasi-pressure defined by (5) and v_{eff} is the effective viscosity defined by (4). v_t and v are turbulent (or eddy) and molecular kinematic viscosities respectively. In Equation (6), k is the turbulent kinetic energy, $\tilde{\epsilon}$ is the rate of dissipation defined below, C_μ is a model constant and f_μ is a damping function introduced to take into account the wall regions.

Equations (1) and (2) are solved in conjunction with the following low Reynolds number k–$\tilde{\epsilon}$ model as proposed by Chien [4]:

$$\overline{u}_k \frac{\partial k}{\partial x_k}=\frac{\partial}{\partial x_k}\left[v+\frac{v_t}{\sigma_k}\frac{\partial k}{\partial x_k}\right]+P-D-\tilde{\epsilon}, \tag{7}$$

$$\overline{u}_k \frac{\partial \tilde{\epsilon}}{\partial x_k}=\frac{\partial}{\partial x_k}\left[v+\frac{v_t}{\sigma_\epsilon}\frac{\partial \tilde{\epsilon}}{\partial x_k}\right]+C_{\epsilon 1}\frac{\tilde{\epsilon}P}{k}-C_{\epsilon 2}f\frac{\tilde{\epsilon}^2}{k}+E, \tag{8}$$

where

$$P=-\overline{u_1'u_1'}\frac{\partial \bar{u}_1}{\partial x_1}-\overline{u_2'u_2'}\frac{\partial \bar{u}_2}{\partial x_2}-\overline{u_1'u_2'}\left(\frac{\partial \bar{u}_1}{\partial x_2}+\frac{\partial \bar{u}_2}{\partial x_1}\right) \tag{9}$$

is the turbulent production and $\overline{u_i'u_j'}$ are the Reynolds stresses that are related to the rate of strain of mean flow

$$\bar{S}_{ij}=\frac{1}{2}\left(\frac{\partial \bar{u}_i}{\partial x_j}+\frac{\partial \bar{u}_j}{\partial x_i}\right) \tag{10}$$

through the following Boussinesq hypothesis,

$$-\overline{u_i'u_j'}=v_t\bar{S}_{ij}-\frac{2}{3}k\,\delta_{ij}. \tag{11}$$

Indeed, the addition of Reynolds stresses (11) to laminar stresses in Navier–Stokes equations introduces the auxiliary terms present in Equations (1) and (2) and redefines the pressure term via Equation (5).

Extra terms D and E, damping functions and model constants, are defined as follows:

$$\epsilon=\tilde{\epsilon}+D, \tag{12}$$

$$D=2v\frac{k}{y^2}, \tag{13}$$

$$E=-2v\frac{\tilde{\epsilon}}{y^2}\exp(-0.5y^+), \tag{14}$$

$$f = 1.0 - 0.22 \exp(-Re_t/6)^2, \tag{15}$$

$$f_\mu = 1.0 - \exp(-0.0115 y^+), \tag{16}$$

c_μ	$c_{\epsilon 1}$	$c_{\epsilon 2}$	σ_k	σ_ϵ
0.09	1.35	1.8	1.0	1.3

In Equations (14)–(16), $Re_t = k^2/\nu\epsilon$ is the turbulent Reynolds number and $y^+ = u_\tau y/\nu$, where u_τ is the friction velocity defined by $u_\tau = \sqrt{\tau/\rho}$, $\tau = \mu(\mathrm{d}u/\mathrm{d}y)$ is the friction and ρ is the density of the fluid; μ is the dynamic viscosity.

3. FINITE ELEMENT DISCRETIZATION

A finite element method is used to discretize Equations (1)–(3) and (7) and (8). Two different finite element formulations are utilized in this study to examine the influence of the formulations on the results. The first method consists of using a standard Galerkin formulation for both Reynolds averaged Navier–Stokes equations (1)–(3) and k–ϵ transport equations (7) and (8). Bilinear elements are employed for velocity components $\bar{u}$, $\bar{v}$ and k–$\tilde{\epsilon}$ variables. Pressure is assumed constant on each element and is eliminated at the element level using a penalty approach. The second method consists of applying a stabilized Galerkin/least-squares (GLS) formulation [9–11] to Equations (1)–(3). This formulation stabilizes the velocity and pressure variables by adding to the Galerkin formulation mesh-dependent terms that are weighted residuals of the original transport equations. Therefore, the GLS method provides a consistent stabilized scheme that allows flows at high Reynolds number or with steep gradients to be solved without encountering numerical instabilities and without accuracy degradation. The GLS method circumvents also the satisfaction of the Babuška–Brezzi (BB) condition (see, Babuška [12] and Brezzi [13]), allowing the implementation of equal-order velocity–pressure elements. In this study, the GLS method has been applied to Equations (1)–(3) employing biquadratic (serendipity) equal-order velocity–pressure elements. k and $\tilde{\epsilon}$ transport equations are solved using a standard Galerkin formulation employing biquadratic (serendipity) elements. The complete details of these formulations for laminar flows are readily available in literature (see e.g. [9–11] and Hannani *et al.* [14]).

A classical Newton–Raphson method was found suitable to linearize the Reynolds averaged equations. For the linearization of the source and sink terms of k and $\tilde{\epsilon}$ transport equations, a method traditionally used with finite volume methods has been used (see Hannani [15] for details of the solution strategy).

3.1. Computational domain, boundary conditions and mesh systems

The computational domain is depicted in Figure 2. The inflow conditions are imposed at a distance of 1.455 m in the upstream of the moving wall, as recommended by Corenflos [7]. The inflow boundary conditions correspond to a pure Poiseuille flow at $Re_q = u_q H/\nu = 5000$, where u_q is the mean bulk velocity and H is the channel height. In a first attempt, experimental profiles are imposed at the inflow. However, experimental k profiles are not very accurate near the walls because of the excessive dimensions of hot wires in wall regions (see Corenflos [7] and Deldicque [16]). Consequently, numerical profiles obtained from a one-dimensional computation of a pure Poiseuille flow are assumed at the inflow, as this leads to a more stable and consistent computation. Computations using experimental and numerical inlet boundary

conditions showed that the developing length is independent of the inlet boundary conditions. No-slip boundary conditions are prescribed for velocity variables ($\bar{u}$, $\bar{v}$), and $k = 0$ and $\tilde{\epsilon} = 0$. In accordance with Corenflos [7] and Deldicque [16], $u_w/u_q = 0.790$, 1.224 and 1.490 for Poiseuille-type, intermediate-type and Couette-type flows respectively. u_w is the moving wall velocity. At the outlet, zero streamwise gradients are assumed for all variables except for $\bar{v}$, which is set to zero.

A moving wall length of 1.38 m ($L \sim 42H$) has been used in the experiment of Corenflos [7]. Preliminary calculations using a moving wall length of $40H$, $90H$ and $120H$ demonstrated that the required length for development depends strongly on the type of flow. Results showed that for the Poiseuille- and intermediate-type flows, a moving wall length of $90H$ (4.4 m) is sufficient to obtain a fully developed flow at the outlet. This is almost twice the length used in the experiment. However, for Couette-type flow, the computation did not produce a fully developed flow at the outlet, even using a moving wall length of $120H$. For each type of flow, one-dimensional calculations are conducted and results are compared with fully developed profiles of two-dimensional calculations. For the Poiseuille-type and intermediate-type flows excellent agreement between 2D and 1D computations are observed. For the Couette-type flow, kinetic energy profiles do not reach to a fully developed condition.

For one-dimensional calculations, three mesh systems of 100 and 180 bilinear elements and 50 biquadratic serendipity elements are used to examine the influence of the mesh size on the solution accuracy. In each case, the first node is situated at $y^+ \sim 0.5$. Complete mesh-independent and element-independent solutions are obtained for the one-dimensional calculations. For two-dimensional developing flows, two mesh systems consisting of 50×100 and 80×100 bilinear elements refined in the wall region and at $x = 1.69$ m (see Figure 3) are used to examine the influence of the mesh system. Computations are conducted using the two different formulations mentioned in Section 3, with comparable mesh systems. A mesh-independent solution is obtained using 80×100 bilinear velocity–constant pressure elements or 40×50 serendipity equal-order velocity–pressure elements. Results are completely independent of the formulation used, except at $x = 1.69$ m due to the stabilizing effects of the GLS method near the discontinuity.

4. RESULTS AND DISCUSSION

Computations are conducted for four different type of flows. First of all, the computational procedure is validated by studying a one-dimensional pure Poiseuille flow at $Re_q = 5000$. Then, two-dimensional Poiseuille-type, intermediate-type and Couette-type flows are studied.

4.1. Pure Poiseuille flow

For a one-dimensional pure Poiseuille flow, the Reynolds averaged equations simplify to

$$\frac{\partial}{\partial y}\left[(\nu + \nu_t)\frac{\partial \bar{u}}{\partial y}\right] = -\frac{2u_\tau^2}{H} = \frac{\partial \bar{p}}{\partial x}. \tag{17}$$

In this case, to start the computations, the friction velocity or pressure gradient is required *a priori*. Friction velocity for the pure Poiseuille flow is measured by Corenflos [7] ($u_\tau = 0.162$ m s^{-1}). However, imposing the experimental friction velocity into Equation (17) is not in general consistent with the turbulence model used for the following reasons. First of all, the experimental friction velocity is often approximate and errors are present during its measure-

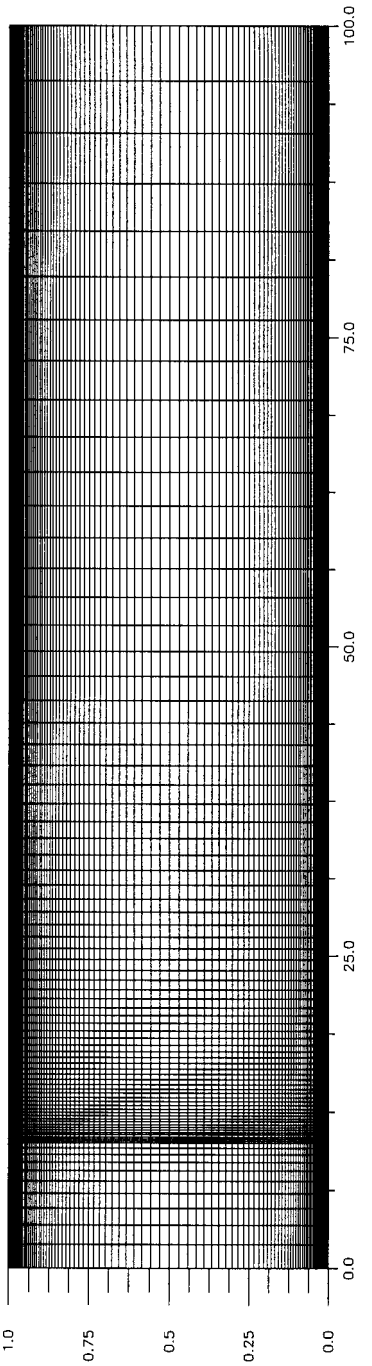

Figure 3. 80×100 bilinear mesh system.

ment and evaluation (see Corenflos [7] and Deldicque [16] for details). Secondly, the friction velocity is indeed the outcome of the computations (by virtue of the velocity profile near the wall) and it depends on the turbulence model used. Therefore, imposing a friction velocity other than the value consistent with the model does not in general preserve the mass flow rate. For symmetric pure Poiseuille flows, imposing the friction velocity does not change other characteristics of the flow. However, for dissymmetric Couette–Poiseuille-type flows, imposing a wrong friction velocity may produce strong modifications of the velocity and k profiles. For example, an intermediate-type flow may change to a Couette-type flow by a slight modification of the input friction velocity (see Hannani [15]). To overcome this difficulty, one can iterate on the friction velocity to obtain a mass flow rate consistent with the experimental results. This method is utilized in this study.

The f_μ damping function of Chien's model (Equation (16)) depends on the friction velocity u_τ and the distance (y) from the wall. For Couette–Poiseuille-type flows at low Reynolds numbers, this definition encounters two difficulties. One is due to the fact that the distance

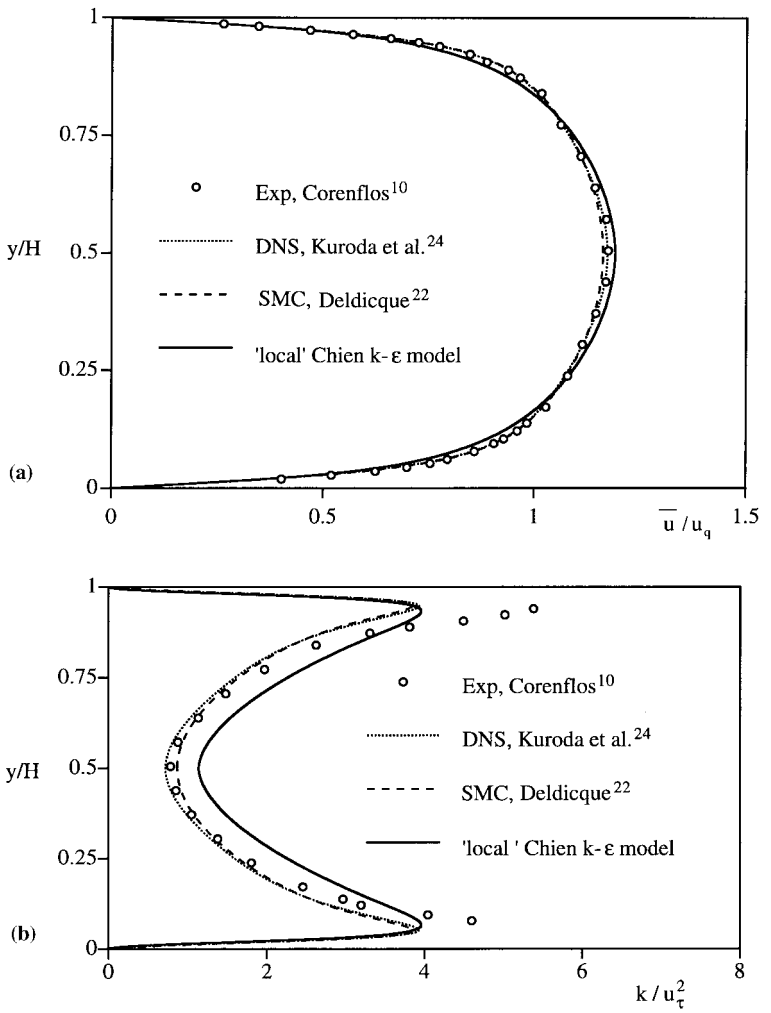

Figure 4. (a) Mean velocity for pure Poiseuille flow; (b) turbulent kinetic energy for pure Poiseuille flow.

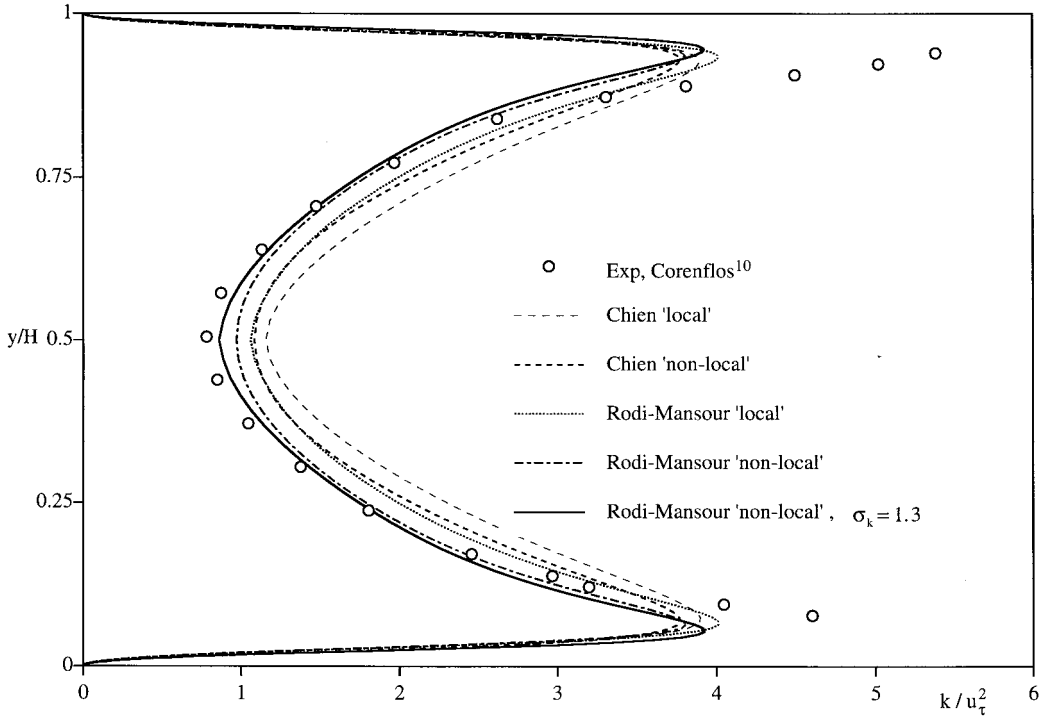

Figure 5. Turbulent kinetic energy for pure Poiseuille flow, influence of f_μ damping function.

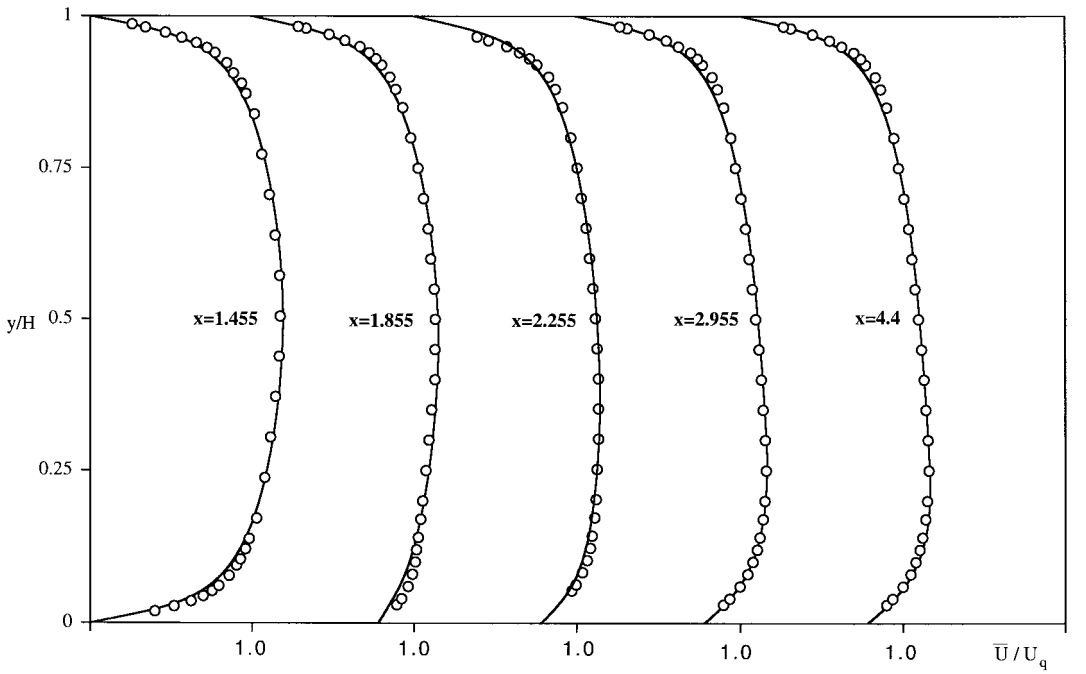

Figure 6. Development of mean velocity for Poiseuille-type flow using Chien model, experimental profile at $x = 2.955$ m is compared with numerical profile at $x = 4.4$ m.

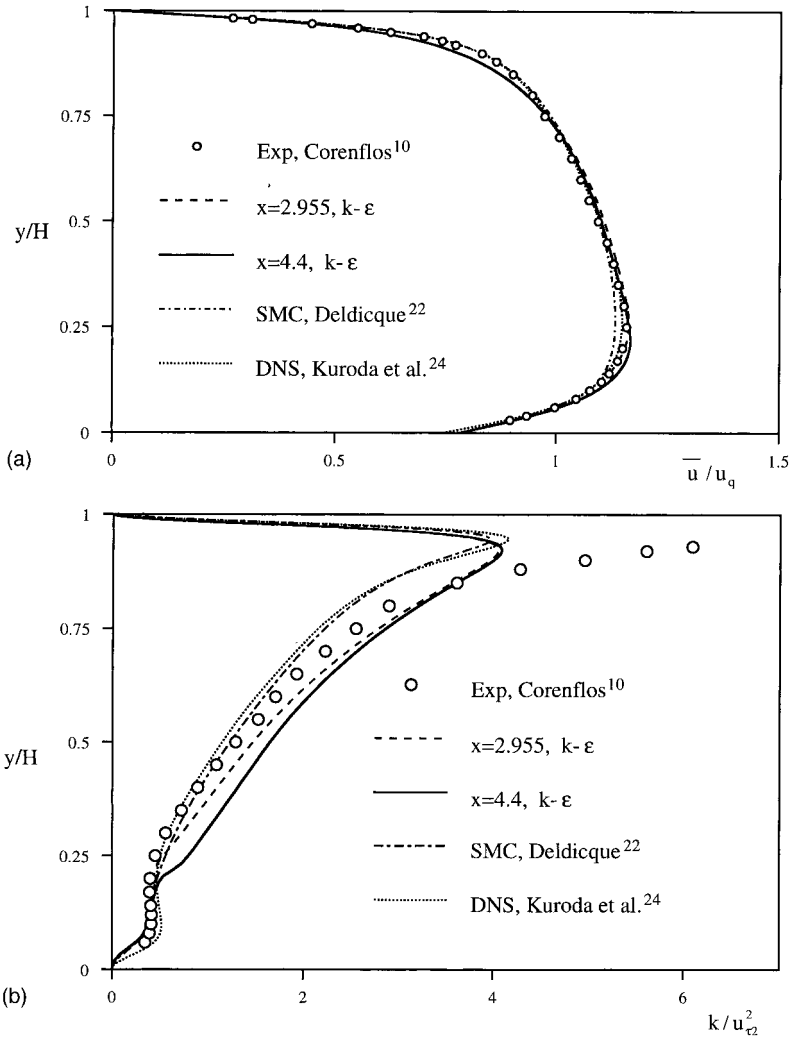

Figure 7. (a) Mean velocity for Poiseuille-type flow; (b) turbulent kinetic energy for Poiseuille-type flow.

from the walls for dissymmetric flows is not clearly defined. Note that for the flows and the Reynolds numbers studied here, the wall region extends up to the central region of the channel. The second problem is due to the fact that the friction velocity vanishes on the moving wall for intermediate-type flow. A solution opted in this study consists of using a local friction velocity for u_τ in (14) and (16). This method is called 'local Chien model' in this paper. In this case, y is the smallest distance from each wall. This section will study the influence of these modifications on the predictions, for the pure Poiseuille flow.

Figure 4(a) and (b) present the mean horizontal velocity ($\bar{u}$) and turbulent kinetic energy (k) for the pure Poiseuille flow using a local Chien model. Results are compared with the measurements of Corenflos and with the DNS data of Kuroda *et al.* [17]. On these figures, the prediction of a second moment closure obtained by Deldicque [16] based on Jakirlic *et al.*'s Reynolds stress model [18] is also shown. Deldicque examined the performance of the models of Jakirlic *et al.* [18], Gibson and Rodi [19] and Shima and Launder [20], by computing

one-dimensional fully developed Couette–Poiseuille flows at $Re = 5000$ and 10000 and concluded that the model of Jakirkic *et al.* provides the best results compared with the experiment. As can be seen from Figure 4(a), the velocity profile obtained by Chien's model is neither in good agreement with the experiment nor with the results of other methods. In addition, the minimum of k at the centre of the channel is overestimated by the k–ϵ model and the peak of k is positioned somewhat farther from the walls than the DNS and SMC predictions (Figure 4(b)). To remedy this behaviour of Chien's k–ϵ model, the authors calculated the f_μ function in (6) using the friction velocity defined classically at walls, called here the 'non-local Chien's model'. In Figure 5, the turbulent kinetic energy profiles are depicted using local Chien and non-local Chien models. One notes that using the wall friction velocity improves the prediction

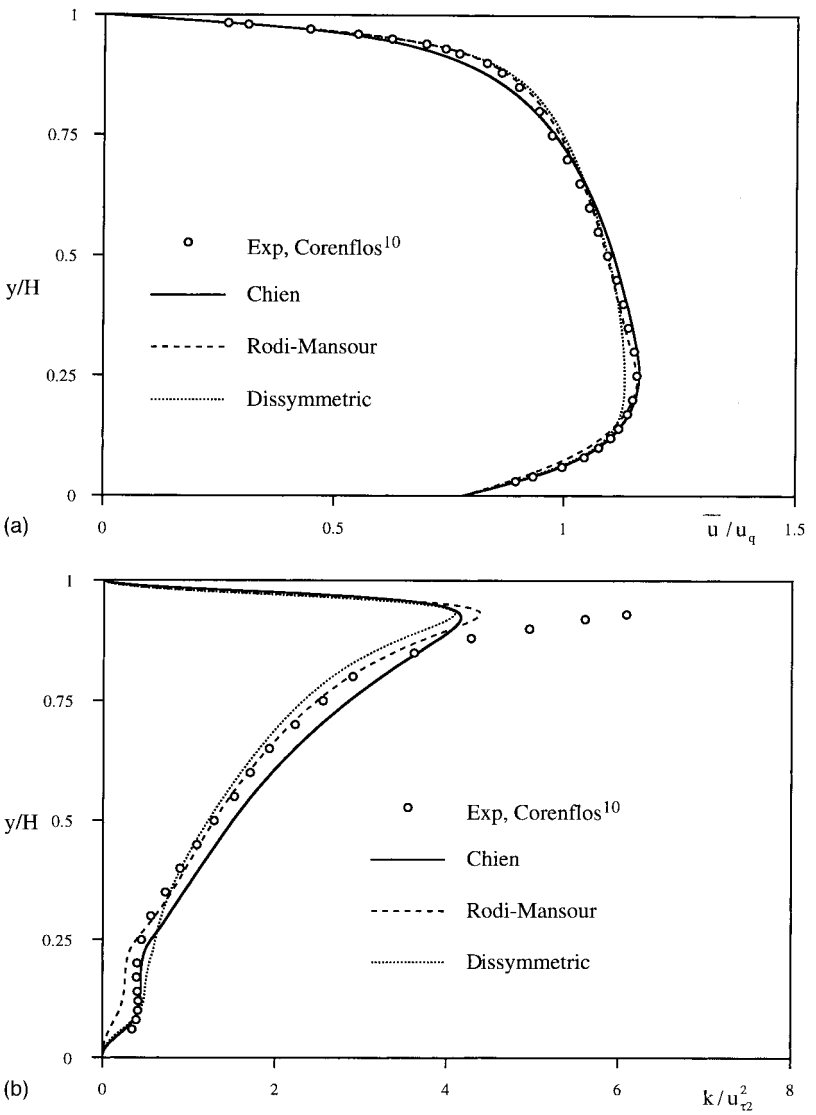

Figure 8. (a) Mean velocity for Poiseuille-type flow, $x = 2.955$ m, influence of f_μ damping function; (b) turbulent kinetic energy for Poiseuille-type flow, $x = 2.955$ m, influence of f_μ damping function.

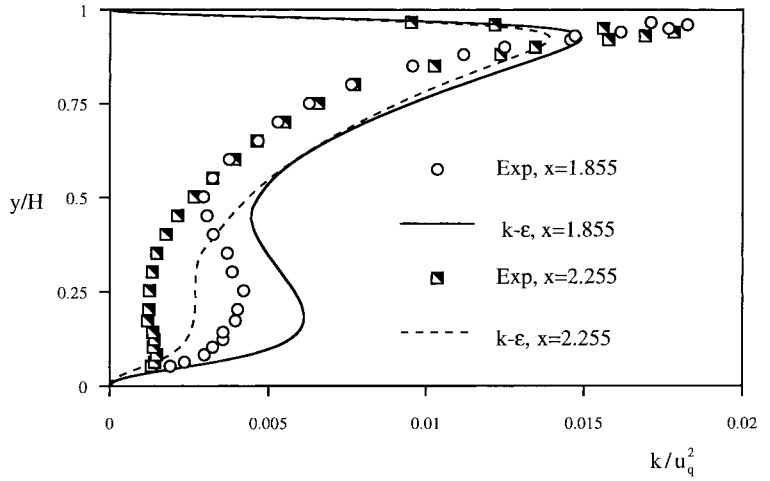

Figure 9. Turbulent kinetic energy profiles at $x = 1.855$ m and $x = 2.225$ m, comparison with experiment.

of k. In a second attempt, the f_μ function of Chien is replaced by the following function proposed by Rodi–Mansour [6], based on DNS data:

$$f_\mu = 1 - \exp(-2 \times 10^{-4} y^+ - 6 \times 10^{-4} y^{+2} + 2.5 \times 10^{-4} y^{+3}). \tag{18}$$

This function leads to improved prediction of k (Figure 5). Indeed, using a non-local friction velocity and also using a function that asymptotes more rapidly to 1 improved results. It can be concluded in this section that for flows at very low Reynolds numbers, the definition of damping functions has a strong influence on the results. This point has a more pronounced effect for dissymmetric Couette–Poiseuille flows (see below).

4.2. Poiseuille-type flow

In Figure 6 the development of the Poiseuille-type flow is shown using a local Chien model. The predictions are globally in good agreement with the experiment, particularly near the outlet. In Figure 7(a) the velocity profiles are compared with the experiment and with SMC and DNS results. One notes that the DNS and SMC are in good agreement with the experimental results in the upper part of the channel, while the k–ϵ model at $x = 2.955$ m behaves correctly in the lower part of the channel. In the upper part, the flow resembles a pure Poiseuille flow and the f_μ function of Chien produces a low level of turbulent viscosity, as observed for the pure Poiseuille flow in Figure 4(a).

k profiles are compared in Figure 7(b). Note that near the upper wall none of the methods are successful in reproducing the experimental curve, due to the excessive dimensions of the hot wires used in Corenflos [7] experiment. One can observe in Figure 7(b) the overestimation of the k level predicted by the k–ϵ model with respect to the SMC curve, in the central region. The same behaviour is found for the pure Poiseuille flow (Figure 4(b)). One notes also in Figure 7(b) the large modification of the k profile between $x = 2.955$ and 4.4 m, indicating that the flow does not reach a fully developed condition at $x = 2.955$ m, the last experimental station.

To investigate the influence of the f_μ function on the results, Rodi–Mansour's [2] f_μ function with a $\sigma_k = 1.3$ and Chien's model using the following dissymmetric definition for distance from the walls are also used in computations.

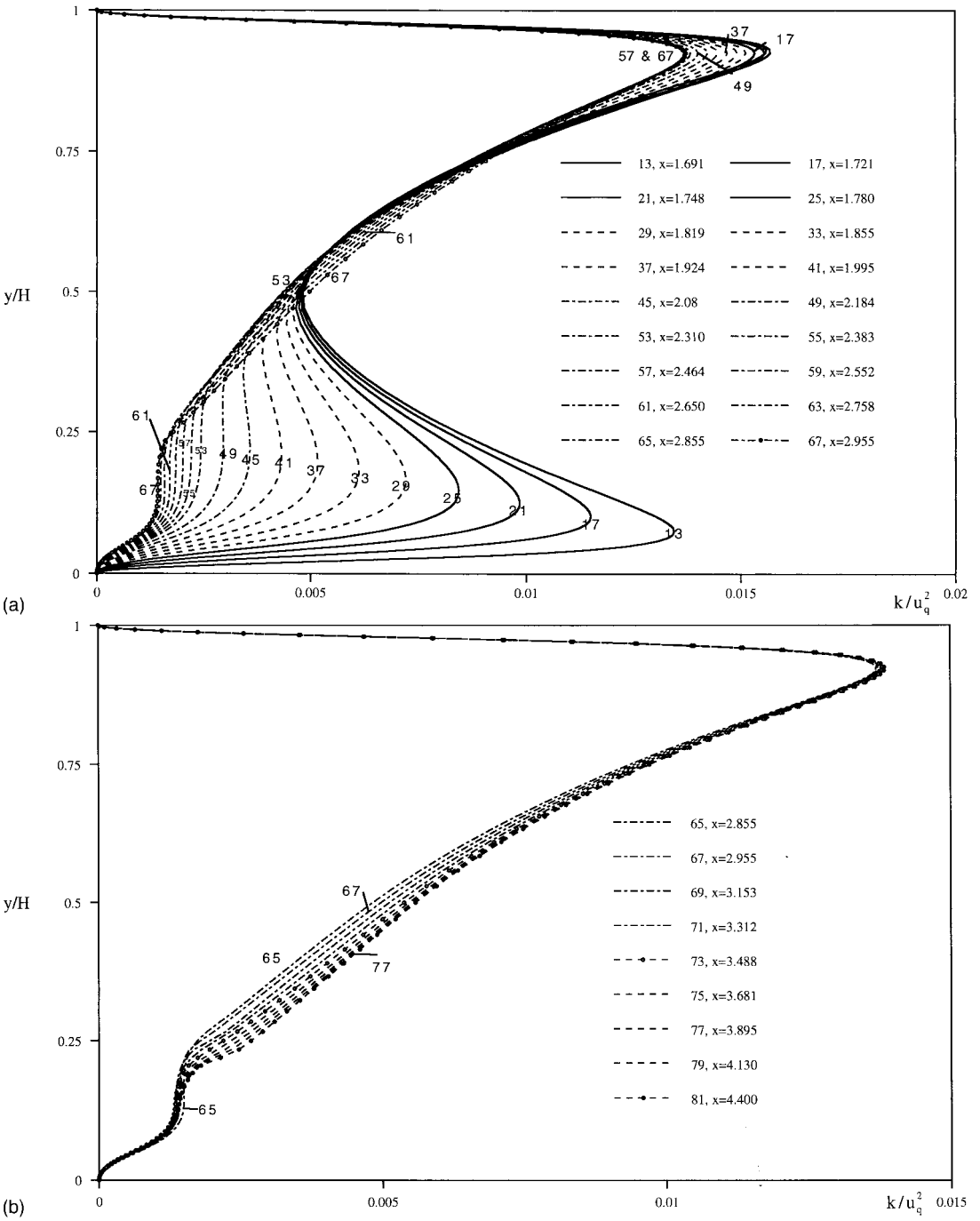

Figure 10. (a) Development of turbulent kinetic energy for Poiseuille-type flow using the Chien model; (b) Development of turbulent kinetic energy for Poiseuille-type flow using the Chien model.

$$\begin{cases} y^+ = \dfrac{u_{\tau 2} \times (H-y)}{\nu}, & \text{if } \mathrm{d}u/\mathrm{d}y < 0 \\ y^+ = \dfrac{u_{\tau 1} \times (y)}{\nu}, & \text{if } \mathrm{d}u/\mathrm{d}y > 0 \end{cases}, \tag{19}$$

where $u_{\tau 1}$ and $u_{\tau 2}$ are the friction velocity of upper and lower walls respectively.

Figure 8(a) and (b) demonstrate that different calibrated f_μ functions would be necessary for k and momentum equations for predicting correctly the velocity and k profiles. Results reveal the drawbacks of eddy viscosity models to solve flows at very low Reynolds numbers. A more rigorous solution consists of modifying the definition of the terms D and E, to take into account the effects of a moving wall with a low level of production in the model.

Kinetic energy profiles are compared with experimental results in Figure 9, for $x = 1.855$ m and $x = 2.225$ m. Unfortunately, the development of the third component of the normal stresses ($\sqrt{\overline{w'^2}}$) has not been measured by Corenflos. Hence, the authors have estimated k as:

$$k_{\exp} = \frac{\overline{u'^2} + 2\overline{v'^2}}{2}. \tag{20}$$

One notes that the predictions are in good agreement qualitatively. Note that this flow is strongly anisotropic (see Corenflos [7]) and the estimation (20) introduces non-negligible errors that make a quantitative comparison difficult.

In Figure 10(a) and (b), the development of k is depicted from $x = 1.69$ m to $x = 4.4$ m. Corenflos observed a two step (two phase) development of the longitudinal turbulence

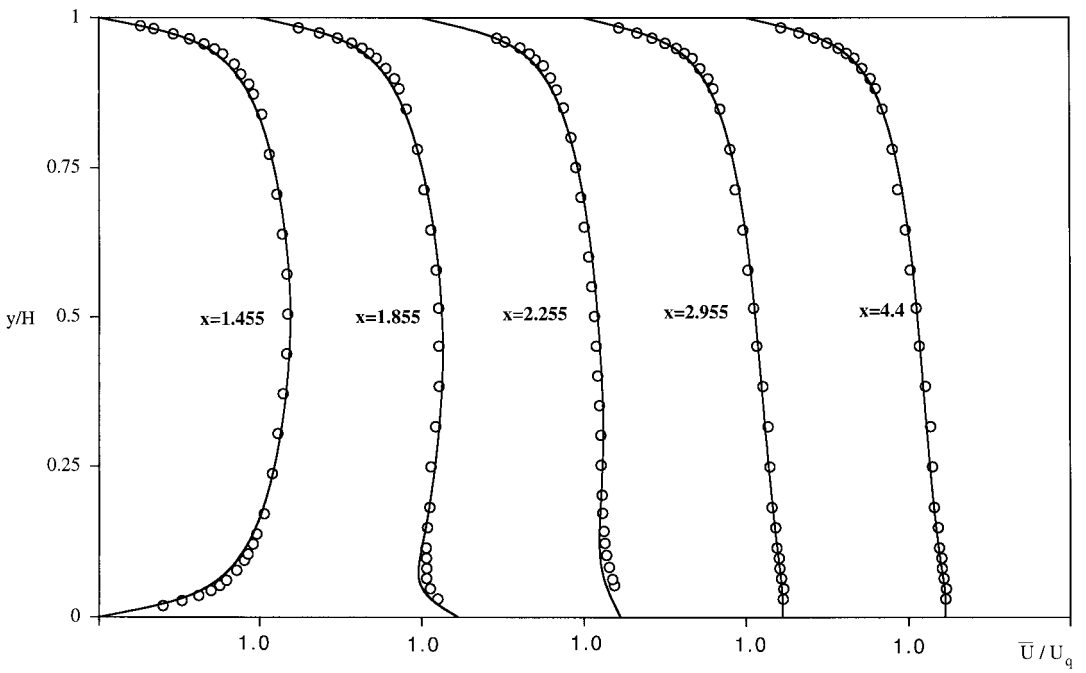

Figure 11. Development of mean velocity for intermediate-type flow using the Chien model, experimental profile at $x = 2.955$ m is compared with numerical profile at $x = 4.4$ m.

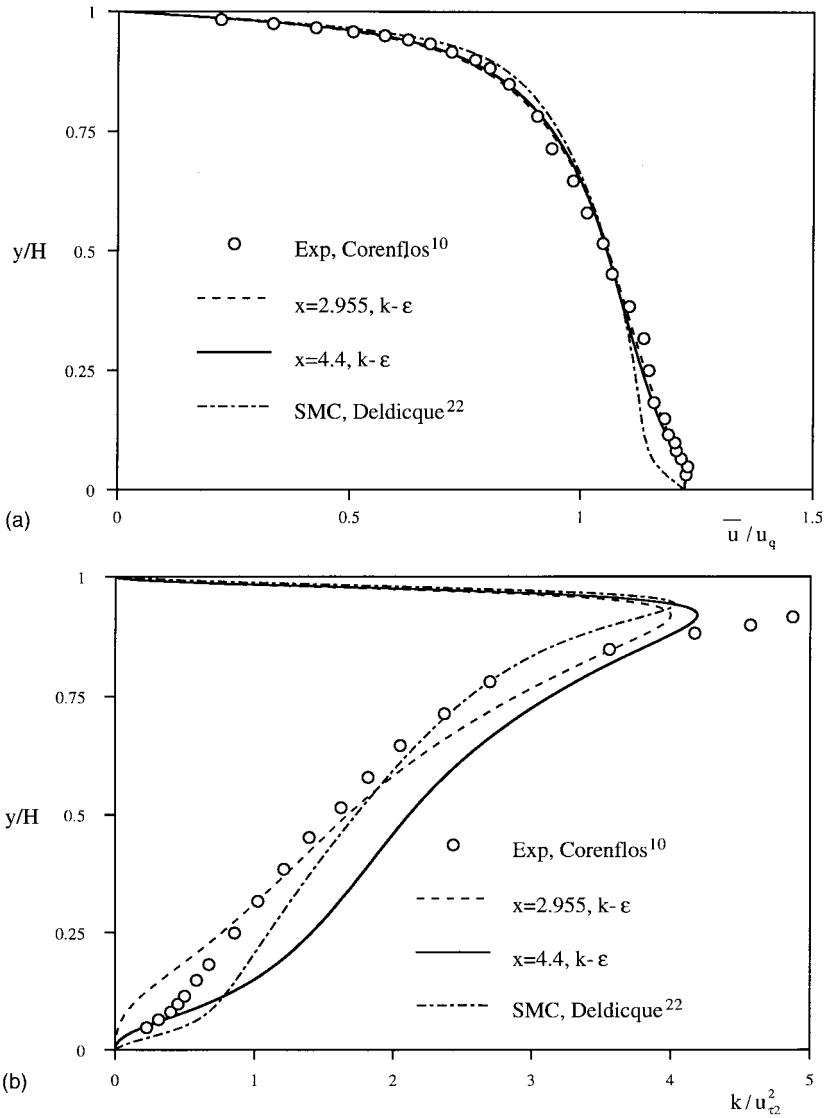

Figure 12. (a) Mean velocity profile for intermediate-type flow; (b) turbulent kinetic energy for intermediate-type flow.

intensity $\sqrt{u'^2}$. First, the peak of $\sqrt{u'^2}$ near the moving wall diminishes very rapidly due to the abrupt decrease of turbulent production. The central region and upper part is not influenced by the change of production near the moving wall. In the second phase, when k reaches its minimum value, the global level of turbulence intensity in the central and upper part increases. One can observe from Figure 10(a) and (b) that the same behaviour is reproduced by the k–ϵ model. In addition, Figure 10(b) shows a very slow development of the turbulent kinetic energy k during the second phase. This point makes it difficult to conclude from the experimental results the full development of the turbulent kinetic energy, because the last two experimental stations are very close to each other ($x = 2.855$ m and 2.955 m respectively).

4.3. Intermediate-type flow

Figure 11 presents the development of the velocity profile using a local Chien model. Results are in good agreement with the experiment, especially at the last section where the computations reproduce a zero slope for the velocity profile at the moving wall. Figure 12(a) and (b) compare the velocity and k profiles with the second moment closure of Jakirlic *et al*. One notes that the SMC predicts a Couette-type flow in this case, and it does not predict correctly the k profile near the moving wall with respect to the experimental curve. One observes also a rather large modification of k profile between ($x = 2.955$ m and $x = 4.4$ m).

Figure 13(a) and (b) show results obtained using Rodi–Mansour's f_μ function and the dissymmetric definition of distance from the walls. An excellent k profile is found for the dissymmetric definition, although the model predicts a Couette-type flow, like the SMC

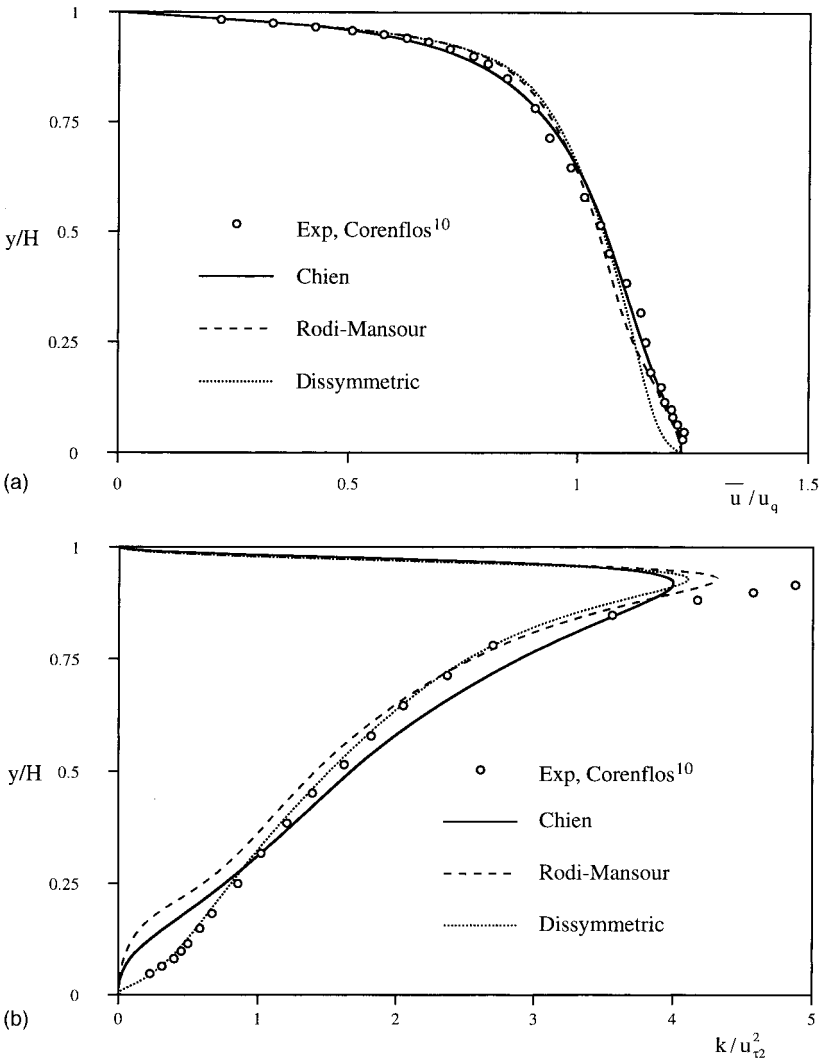

Figure 13. (a) Mean velocity for intermediate-type flow, $x = 2.955$ m, influence of f_μ damping function; (b) turbulent kinetic energy for intermediate-type flow, $x = 2.955$ m, influence of f_μ damping function.

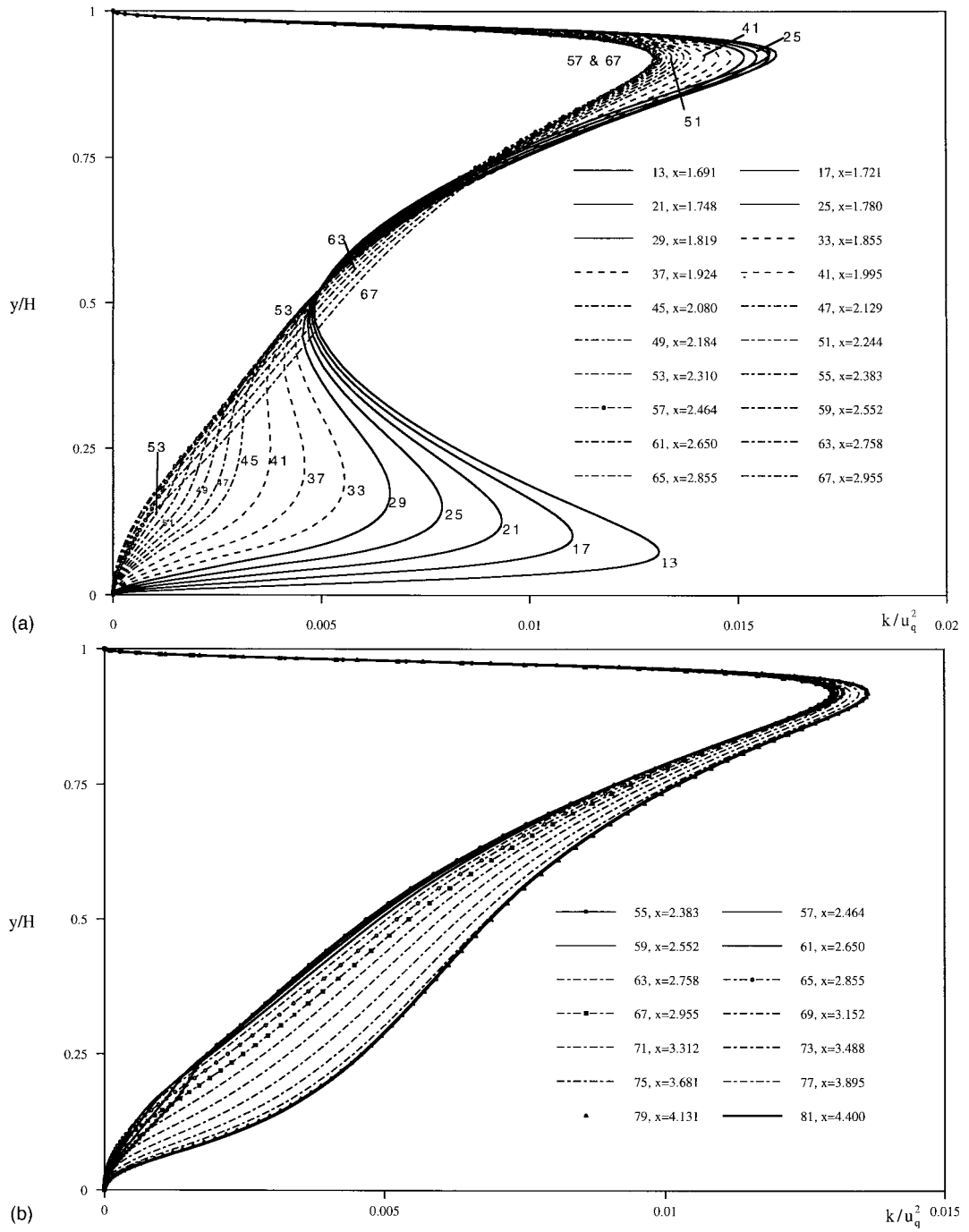

Figure 14. (a) Development of turbulent kinetic energy for intermediate-type flow using the Chien model; (b) development of turbulent kinetic energy for intermediate-type flow using the Chien model.

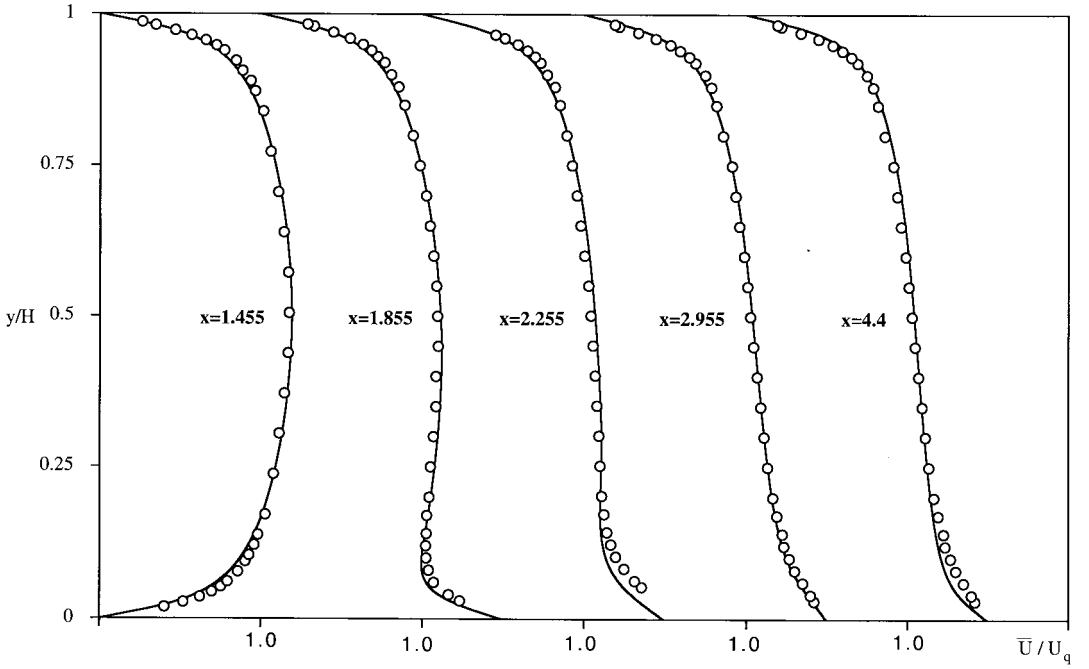

Figure 15. Development of mean velocity for Couette-type flow using the Chien model, experimental profile at $x = 2.955$ m is compared with numerical profile at $x = 4.4$ m.

prediction. Therefore, the same conclusion as the Poiseuille-type flow case can be drawn here. Results reveal the importance of the definition of the f_μ function and the need to calibrate the near-wall treatments for a flow near a moving wall with zero shear stress.

In Figure 14(a) and (b), the development of k is depicted from $x = 1.69$ m to x = 4.4 m. A two phase development of k is found as for the Poiseuille-type flow.

4.4. Couette-type flow

Figure 15 presents the development of velocity profile using a local Chien model. It can be seen that the velocity profile does not reach a fully developed condition at the last experimental station. Deldicque states in his dissertation that he cannot ensure the full development of the experimental $\sqrt{u'^2}$. Figure 16(a) and (b) compare the velocity and k profiles with the experiment and SMC predictions. SMC agrees well with the experiment. However, if the uncertainity concerning the full development of experimental k profiles is taken into account, the SMC result is certainly not convincing. In addition, the SCM velocity profile is not in close agreement with the experiment. It is noted that rather large differences between the k–ϵ model's kinetic energy profile and the experimental curve near the moving wall. The authors attribute the difference partly to the model's deficiency near the moving wall and partly to the fact that the model predicts perhaps a slower development compared with the experiment. Experimental studies with a longer channel need to be conducted to elucidate this point.

In Figure 17(a) and (b), the development of k profiles is depicted from $x = 1.69$ m to $x = 4.4$ m. A two phase development of k is found as for the Poiseuille-type and intermediate-type flow. Comparing Figures 10, 14 and 17, one observes that the developing length is a function of the moving wall velocity.

5. CONCLUSION

Developing Couette–Poiseuille flows have been studied in this work using the low Reynolds number k–ϵ model of Chien. Attention is devoted to obtain mesh-independent solutions and to check the full development of flows, using different grid systems and different channel lengths. Two different finite element formulations have been employed to examine the influence of the discretization method on the results. Computations revealed the drawbacks of an eddy viscosity model to predict correctly dissymmetric flows at a low Reynolds number of 5000. In summary, the results are strongly influenced by the definition of the damping function f_μ, which controls the level of turbulent viscosity in the flow. In order to reproduce the experimental profiles, highly tuned and calibrated k–ϵ near-wall treatments would be neces-

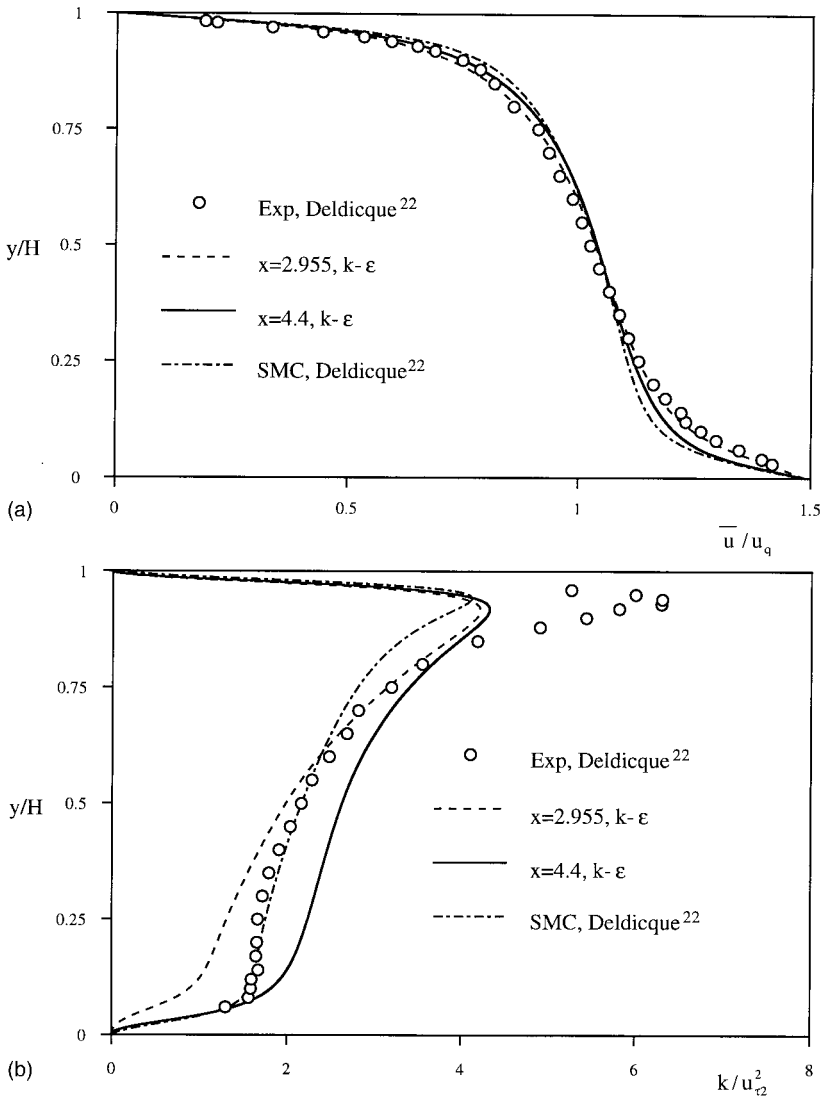

Figure 16. (a) Mean velocity profile for Couette-type flow; (b) turbulent kinetic energy for Couette-type flow.

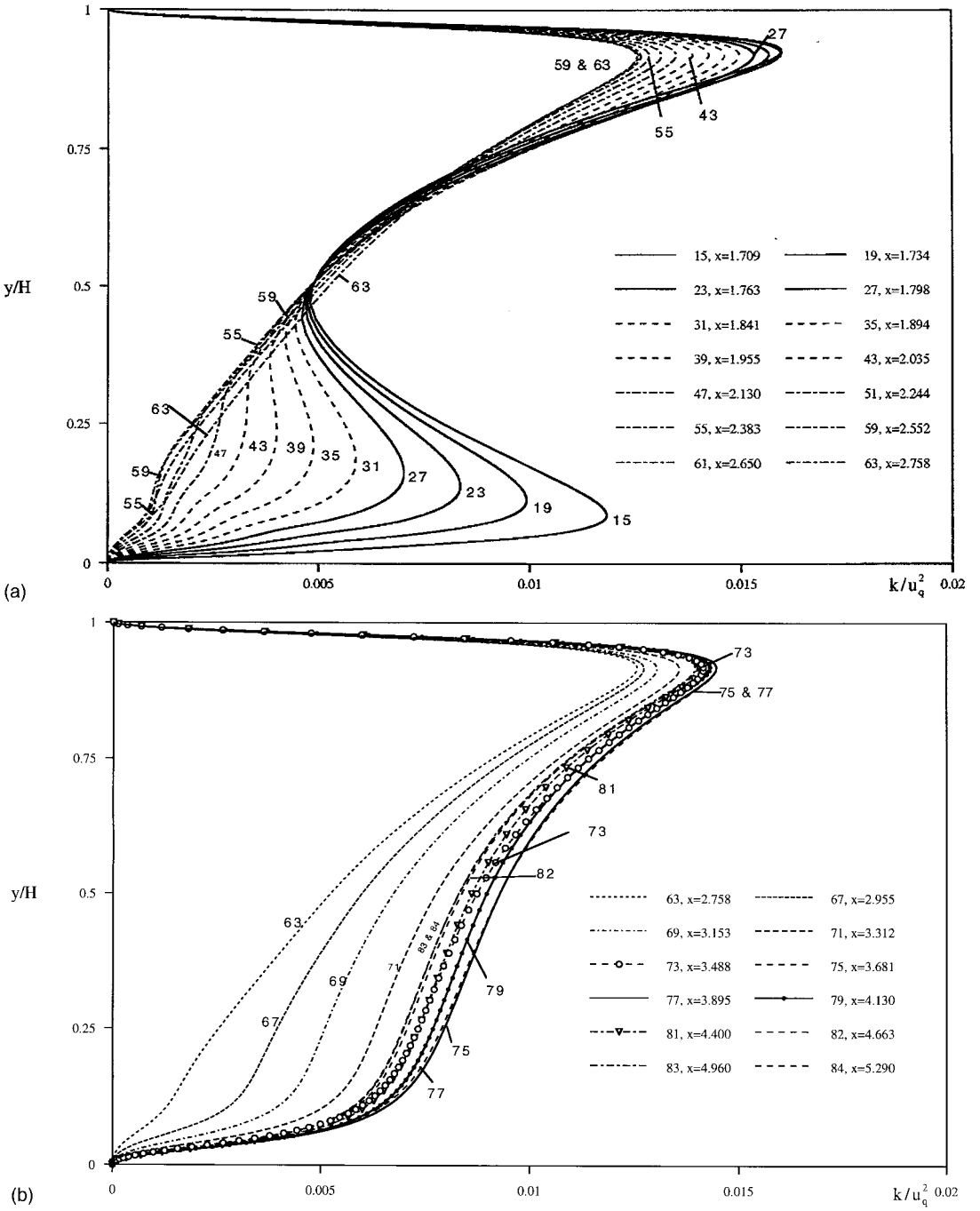

Figure 17. (a) Development of turbulent kinetic energy for Couette-type flow using the Chien model; (b) development of turbulent kinetic energy for Couette-type flow using Chien model.

sary for each type of flow. Recourse to higher level closures, such as k–ϵ–v' models that do not require an eddy viscosity assumption might be a better solution. Research is in progress to investigate the effects of a k–ϵ–v' model on predictions. Rodi–Mansour's complete k–ϵ model, which is based on the DNS data of a fully developed symmetric Poiseuille flow, needs also to be studied in a subsequent work. However, Chien's k–$\tilde{\epsilon}$ model behaves rather well in reproducing essential features of these flows, such as a two phase development of k profiles and a strong dependence of the moving wall velocity on the developing length. For the Couette-type flow case, using a moving wall length two times longer than the length used in the experimental study did not lead to a fully developed flow. Experimental work with a longer channel might be necessary to explain such a slow development of Couette–Poiseuille flows.

REFERENCES

1. V.G. Patel, W. Rodi and G. Scheurer, 'Turbulence models for near-wall and low Reynolds number flows: A review', *AIAA J.*, **23**, 1308–1319 (1985).
2. W. Rodi and N.N. Mansour, 'Low Reynolds number k–ϵ modeling with the aid of direct simulation data', *J.F.M.*, **250**, 509–529 (1993).
3. V. Michelassi, W. Rodi and J. Zhu, 'Testing a low Reynolds number k–ϵ turbulence model based on direct simulation data', *Eng. Notes*, *AIAA J.*, **31**, 1720–1723 (1993).
4. K.Y. Chien, 'Prediction of channel and boundary layer flows with a low Reynolds number turbulence model', *AIAA J.*, **20**, 33–38 (1982).
5. J.C. Monnier, 'Hydrodynamics des écoulements turbulents dans les cellules d'électrodéposition', *Thèse de doctoral*, *No. 358*, Université des Sciences et Techniques de Lille Flandres et Artois, Villeneuve d'Ascq, France, 1989.
6. J.C. Monnier and M. Stanislas, 'Critical examination of various turbulence models applied to different one dimensional internal flows, including Couette flows with pressure gradient', in C. Taylor, P.M. Gresho, R.L. Sani and J. Hauser (eds.), *Numerical Methods in Laminar and Turbulent Flows*, vol. **6**, part 1, Pineridge Press, Swansea, 1989, pp. 297–306.
7. K. Corenflos, 'Etude expérimentale d'écoulements de Couette–Poiseuille turbulent à faible nombre de Reynolds', *Thèse de Doctorat*, *No. 1013*, Université des Sciences et Techniques de Lille Flandres et Artois, Villeneuve d'Ascq, France, 1993.
8. *ERCOFTAC Workshop on Data Bases and Testing of Calculation Methods for Turbulent Flows*, April 3–7, 1995, University of Karlsruhe, Karlsruhe, Germany, 1995.
9. A.N. Brooks and T.J.R. Hughes, 'Streamline upwind/Petrov–Galerkin formulation for convection dominated flows with particular emphasis on the incompressible Navier–Stokes equation', *Comput. Methods Appl. Mech. Eng.*, **32**, 199–259 (1982).
10. T.J.R. Hughes, L.P. Franca and G.M. Hulbert, 'A new finite element formulation for computational fluid dynamics: VIII The Galerkin/least-squares method for advective–diffusive equations', *Comput. Method Appl. Mech. Eng.*, **73**, 173–189 (1989).
11. L.P. Franca and S.L. Frey, 'Stabilized finite element methods: II. The incompressible Navier–Stokes equations', *Comput. Methods Appl. Mech. Eng.*, **99**, 209–233 (1992).
12. I. Babuška, 'The finite elements with Lagrangian multipliers', *Numer. Math.*, **20**, 179–192 (1973).
13. F. Brezzi, 'On the existence, uniqueness and approximation of saddle point problems arising from Lagrange multipliers', *Rev. française Automatique Informatique Recherche Opèrationnelle*, *Ser. Rouge Anal. Numér.*, **8**, 129–151 (1974).
14. S.K. Hannani, M. Stanislas and P. Dupont, 'Incompressible Navier–Stokes computations using SUPG and GLS formulations—A comparison study', *Comput. Methods Appl. Mech. Eng.*, **124**, 153–170 (1995).
15. S.K. Hannani, 'Calcul d'écoulement laminaires et turbulents par une méthode d'élements finis: Influence de la formulation', *Thèse de Doctorat*, *No. 1745*, Université des Sciences et Techniques de Lille Flandres et Artois, Villeneuve d'Ascq, France, 1996.
16. A. Deldicque, 'Etude de l'influence du nombre de Reynolds sur des écoulements turbulents de Couette–Poiseuille a l'aide d'une approche expérimentale et d'une modélisation aux contraintes de Reynolds', *Thèse de Doctorat*, *No. 1313*, Université des Sciences et Techniques de Lille Flandres et Artois, Villeneuve d'Ascq, France, 1995.
17. A. Kuroda, N. Kasagi and A. Hirta, 'Direct numerical simulation of turbulent plane Couette–Poiseuille flows: effect of mean shear on the wall turbulence structures', *Ninth Symposium on Turbulent Shear Flows*, Kyoto, Japan, August, 1993, pp. 8.4.1–8.4.6.
18. S. Jakirlic, K. Hanjalic and F. Durst, 'Computation of accelerating 3D turbulent boundary layers by a second moment closure', in *Refind Flow Modelling and Turbulence Measurements*, *Proceedings of 5th International Symposium*, Paris, September 7–l0, 1993, pp. 57–64.
19. M.M. Gibson and W. Rodi, 'Simulation of free-surface effects on turbulence with a Reynolds stress model', *J. Hydraul. Res.*, **27**, 233–244 (1989).
20. N. Shima and B.E. Launder, 'Second moment closure for the near wall sublayer: developments and applications', *AIAA J.*, **27**, 1319–1325 (1989).

